Theor Appl Climatol
DOI 10.1007/s00704-017-2205-7

ORIGINAL PAPER

A remarkable climate warming hiatus over Northeast China since 1998

Xiubao Sun[1,2,3] · Guoyu Ren[2,3] · Yuyu Ren[3] · Yihe Fang[4] · Yulian Liu[5] · Xiaoying Xue[2] · Panfeng Zhang[2]

Received: 30 November 2016 / Accepted: 18 June 2017

Abstract Characteristics and causes of global warming hiatus (GWH) phenomenon have received much attention in recent years. Monthly mean data of land surface air maximum temperature (Tmax), minimum temperature (Tmin), and mean temperature (Tmean) of 118 national stations since 1951 in Northeast China are used in this paper to analyze the changes of land surface air temperature in recent 64 years with an emphasis on the GWH period. The results show that (1) from 1951 to 2014, the warming trends of Tmax, Tmin, and Tmean are 0.20, 0.42, and 0.34 °C/decade respectively for the whole area, with the warming rate of Tmin about two times of Tmax, and the upward trend of Tmean obviously higher than mainland China and global averages; (2) in the period 1998–2014, the annual mean temperature consistently exhibits a cooling phenomenon in Northeast China, and the trends of Tmax, Tmin, and Tmean are −0.36, −0.14, and −0.28 °C/decade respectively; (3) in the GWH period, seasonal mean cooling mainly occurs in northern winter (DJF) and spring (MAM), but northern summer (JJA) and autumn (SON) still experience a warming, implying that the annual mean temperature decrease is controlled by the remarkable cooling of winter and spring; (4) compared to the global and mainland China averages, the hiatus phenomenon is more evident in Northeast China, and the cooling trends are more obvious in the cold season; (5) the Northeast China cooling trend occurs under the circulation background of the negative phase Arctic Oscillation (AO), and it is also closely related to strengthening of the Siberia High (SH) and the East Asian Trough (EAT), and the stronger East Asian winter monsoon (EAWM) over the GWH period.

✉ Guoyu Ren
guoyoo@cma.gov.cn

1 College of Atmospheric Science, Nanjing University of Information Science &Technology, Nanjing 210044, China

2 Department of Atmospheric Science, School of Environmental Studies, China University of Geosciences, Wuhan 430074, China

3 Laboratory for Climate Studies, National Climate Center, China Meteorological Administration, Beijing 100081, China

4 Liaoning Meteorological Bureau, Shenyang 110001, China

5 Heilongjiang Meteorological Bureau, Haerbin 150001, China

1 Introduction

Intergovernmental Panel on Climate Change (IPCC) fifth assessment report indicated that the global land surface is warming at a rate of 0.095–0.107 °C/decade during 1901–2012 (Stocker et al. 2013). Global warming is therefore a consensus in climatological community. However, Cater (2006) found that global warming appears to stop or slow down since 1998. Easterling and Wehner (2009) analyzed the observational data and indicated that the global land surface air temperature is not significantly warming as expected during the last decade, with some areas even cooling, and this phenomenon is called global warming hiatus (GWH). The GWH, in both global and regional scales, has received a widespread concern in the last years (e.g., Kerr 2009; Franzke 2014; Fyfe and Gillett 2014; Li et al. 2015; An et al. 2016). By analyzing the seasonal characteristics of the GWH, Kosaka and Xie (2013) and Trenberth et al. (2014b) found that the warming trends in the northern hemisphere significantly slowdown in winter but continually increase in summer. A recent analysis showed that the GWH mainly appears in the low and middle latitudes of global lands, with surface air temperature

Published online: 05 July 2017

at most stations there witnessing a stable or decreased trend after 1998 (Sun et al. 2017). However, further studies revealed that the GWH seems not detectable in change of global extreme temperature event frequency all the time (Seneviratne et al. 2014). Karl et al. (2015), based on a new land and ocean dataset, recently also indicated that global surface and land surface warming had never slowed down, challenging the existence of the GWH.

In recent years, however, more researchers confirmed the GWH phenomenon on global and regional scales, and many works were focused on the possible reasons of the GWH (Fyfe et al. 2016). A number of studies indicated that the mechanisms of the GWH may be related to the external forcing and natural variability. The influence from external forcing may include the prolonged solar minimum (Hansen et al. 2011), the increased volcanic eruptions (Balmaseda et al. 2013; Santer et al. 2014), the reduced water vapor in stratospheric (Solomon et al. 2010, 2011), and the increased emissions of anthropogenic aerosols (Lean and Rind 2009). On the other hand, mechanisms of the natural variability proposed to explain the GWH phenomenon include the increased ocean heat uptake especially the layer below 700 m (e.g., Chen and Tung 2014; Hansen et al. 2011; Meehl et al. 2013; Trenberth et al. 2014a), the cool waters of the equatorial Pacific surface (Kosaka and Xie 2013), and the Pacific Decadal Oscillation (PDO) into the negative phase since 1998 (Tollefson 2014). Several recent studies have attributed the GWH to the 60-year-quasi-periodic natural climate variability and have provided a theoretical framework for the dynamical processes and the decadal-scale prediction of temperature variation. Li et al. (2013a, b) indicated that North Atlantic Oscillation (NAO) leads the multidecadal variability in Northern Hemispheric surface temperature by about 15–20 years through a delayed effect on the North Atlantic Ocean, and the recent NAO decadal weakening can be a useful predictor of the hiatus in both Atlantic Multidecadal Oscillation (AMO) and Northern Hemispheric mean surface temperature. Sun et al. (2015) proposed a new "delayed oscillator theory" of the North Atlantic decadal-scale air-sea coupling to understand the underlying physical mechanisms of the 60-year-quasi-periodic natural climate variability.

For mainland China, annual mean temperature anomalies remains at a high level since 2001, but the warming trend has also slowed down (Tang et al. 2012). Li et al. (2015) found that the annual mean maximum temperature (Tmax) increasing trend had slowed down in mainland China since 1998, and although the Tmax significantly increased in summer (JJA), the trend of minimum temperature (Tmin) obviously decreased in winter (DJF). Yan and Liu (2014) indicated that most of the Tibetan Plateau still showed strong warming trend since 1998. Recently, based on the ice-core record, An et al. (2016) also founded a remarkable cooling phenomenon in northwestern Tibetan Plateau region.

Northeast China has been one of the most significant warming regions in mainland China and East Asia for the last more than five decades (Ren et al. 2012; Sun et al. 2016). Investigation into the spatial and temporal patterns of the long-term land surface air temperature change during the GWH period in Northeast China will help in understanding of the climate forcing mechanism of the larger-scale GWH. Furthermore, the Northeast China Plain is one of the most productive regions of grain in the world. The grain yield in this region amounts to ~20% of China's total. Previous studies found that the crop production has strong dependence on the growth season mean temperature and heat conditions (Lobell et al. 2011). The cooling of the warm season will probably increase the instability of agricultural production in Northeast China (Jin et al. 2002; Liu et al. 2013a, b). It is thus also important to understand the characteristics of annual and the warm-season temperature changes in the GWH period in Northeast China, and to predict the future change in surface air temperature and heat condition so that an adaption strategy can be developed to reduce the risk of the summer low temperature disasters.

In this paper, we analyze the changes in Northeast China land surface air temperature in recent 64 years, with an emphasis on the GWH period. The paper is organized as follows. We describe the data and methods used in this paper in Section 2 after the introduction. Results of the analysis are presented in Section 3. A brief analysis of circulation background of the warming slowdown is offered in Section 4. We offer a discussion of the results in Section 5. Finally, main conclusions are presented in Section 6.

2 Data and methods

2.1 Data sources and study region

The source of the monthly mean measurements used in our current analysis is the China Homogenized Historical Temperature Dataset (CHHTD-V1.0), including 2419 stations, with a record length of 64 years (1951–2014), which included a quality control and homogenization procedure (Cao et al. 2016). The inhomogeneity problem can be considered to have little influence on the dataset. The study area comprises the east region of Inner Mongolia, Liaoning, Heilongjiang, and Jilin provinces in Northeast China. In this paper, we initially selected only those national stations that had at least 70% data coverage since

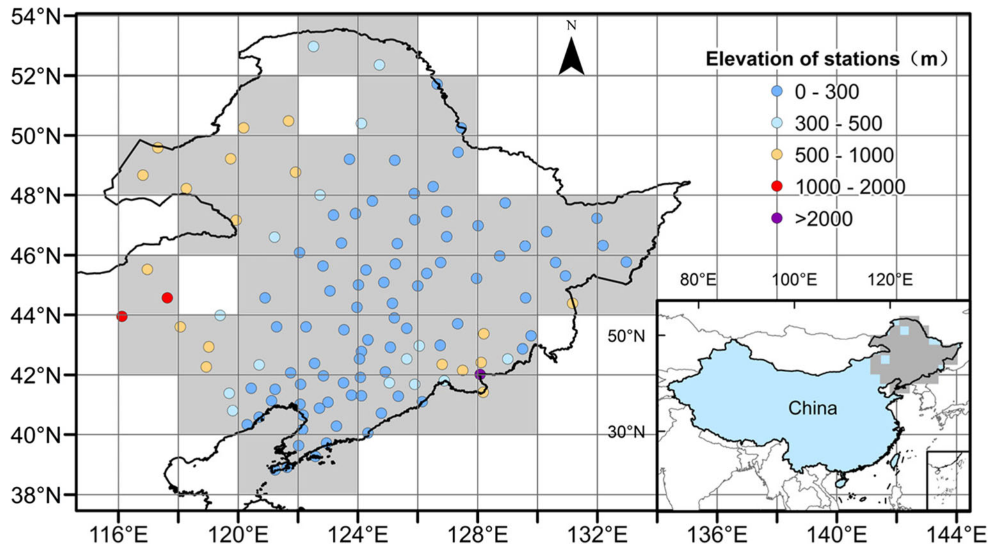

Fig. 1 Map of study region (*gray shade in bottom right corner*) and location of 118 stations (*various color points*). The elevation of stations is indicated by the different colors. The *grid boxes* at a spatial resolution of 2° × 2°used for the estimation of regional average are shown by the *gray areas*

1951 and at least 20 years of records in the base period 1961–1990 in the study region. We mainly focused on the hiatus phenomenon, and therefore we removed the stations with records of less than 15 years in length in the GWH period. We also considered the problem of missing data by discarding the annual (season) value with monthly records less than 8 (3) months in calculating annual (seasonal) temperature anomalies. Finally, we obtained a dataset consisting of 118 stations across the study area for use in our analysis. There were only 26 stations in 1951, the number increased to 70 in 1955, and substantially increased to 118 after 1960. The study region (gray areas), station distribution (various color points), and the altitudes of the stations are shown in Fig. 1.

This study utilized six circulation indices to analyze the abnormal characteristics of the atmospheric general circulation (Section 4). The monthly mean indices were from the National Climate Center (NCC) of the China Meteorological Administration (CMA), which were managed and regularly updated by the Climate Diagnostics and Prediction Division of the NCC. The National Center for Environmental Prediction/National Center for Atmospheric Research (NCEP/NCAR) reanalysis data, including the monthly wind, sea-level pressure (SLP), and geopotential heights at 500 hPa and 1000 hPa since 1951 with a spatial resolution of 2.5° × 2.5°, were used for calculating the indices.

2.2 Methods

We constructed regional series by the reference method of Jones et al. (2001). Firstly, the study area was divided into a total of 42 grid boxes with the spatial resolution of 2° × 2°, and each grid boxes had at least one station as shown in Fig. 1 (gray areas). Then, gridding of the temperature anomalies are made by averaging all values within 2° × 2° grid boxes. Finally, the time series were constructed by area-weight averaging all the grid boxes with data using the cosines of the central latitudes of the grid boxes as weight coefficients.

The analysis used 1961–1990 as the base period, mainly because of the better spatial coverage of stations in the period, and the comparability with previous studies for surface air temperature. China lies in the northern hemisphere, and therefore seasons were divided into spring (MAM), summer (JJA), autumn (SON) and winter (DJF, December to February of the following year). Annual mean values were those from January to December.

The linear trends of the anomaly series were obtained by using least squares method to calculate the linear regression coefficients between temperature and ordinal numbers of time (e.g., $i = 1, 2, 3…64$ for 1951–2014). The significance of the linear trends of temperature series was judged by using two-tailed student's t test method. In this study, a trend was considered to be statistically significant if it is significant at the 5% ($P < 0.05$) level. We also used a nonparametric Kendall's tau based Sen's slope estimator (Sen 1968) to calculate trends, since this method does not assume a distribution for the residuals and is robust to the effect of outliers in the series, and it has been widely used in the studies of hydrological and extreme climate change (e.g., Alexander et al. 2006; Zhao et al. 2016; Kosaka and Xie 2013). The significance of the Sen's slope is judged by using Mann-Kendall test method (Kosaka and Xie 2013; Zhao et al. 2016).

In Section 4, empirical orthogonal function (EOF) (Lorenz 1956) and singular value decomposition (SVD) method (Golub and Reinsch 1970; Lathauwer et al. 2000) were used to analyze the possible influence of the

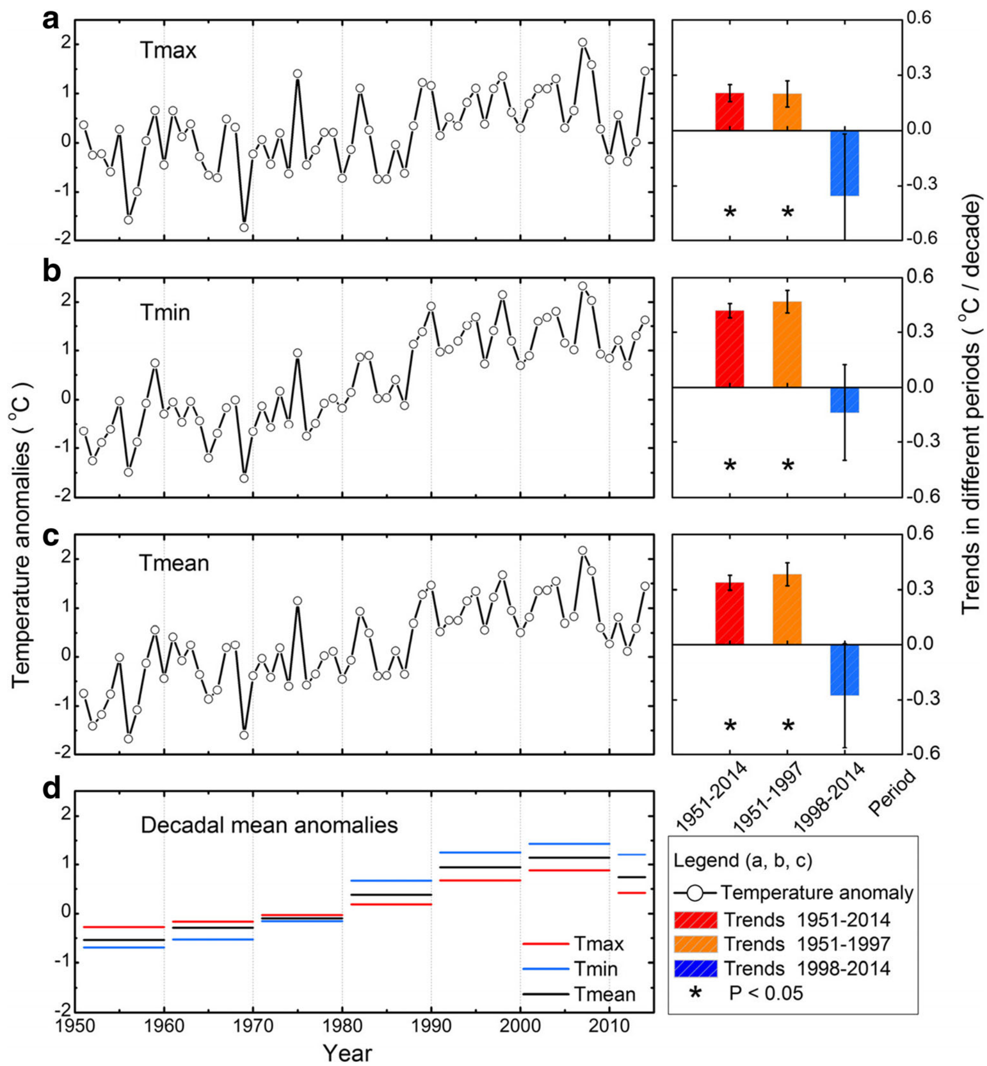

Fig. 2 Linear trends of temperature series for different periods (1951–2014, 1951–1997, and 1998–2014). Figure on the *left* shows the annual mean time series (°C, *black lines*) of Tmax (**a**), Tmin (**b**), and Tmean (**c**), anomalies relative to 1961–1990. Figure on the *right* shows the linear trends for the period 1951–2014 (°C/decade, *red bars*), 1951–1997 (°C/decade, *orange bars*), and 1998–2014 (°C/10 years, *blue bars*). Error bars indicate two times the standard deviation. Statistically significant ($P < 0.05$) trends are marked with *asterisks*. Figure on the *bottom* shows the interdecadal mean temperature anomalies of Tmax (*red lines*), Tmin (*blue lines*), and Tmean (*black lines*) (**d**)

circulation factors on the observed temperature change in Northeast China.

2.3 Circulation indices

We used six circulation indices in Section 4, and their definitions are as follows:

Arctic Oscillation (AO) index (I_{AO}): normalized time coefficient series of the EOF1 of 1000 hPa height anomaly field (relative to the 1981–2010) (20–90° N) (Thompson and Wallace 1998).

Siberia High (SH) index (I_{SH}): winter mean sea level pressure anomaly (relative to 1981–2010) in SH region (45–70° N, 80–110° E). The index is the normalized value.

East Asian Trough (EAT) index (I_{EAT}): difference between the maximum height and the minimum height on the 500 hPa geopotential heights in the area of 110–170° E and 30–55° N.

Station of the East Asian trough (I_{EATS}): the mean position of the EAT line on the 500 hPa geopotential heights in the area of 110–170° E and 30–55° N.

East Asian winter monsoon (EAWM) strength index (I_{EAWM}) (Zhu et al. 2008):

$$I_{EAWM} = \overline{U}_{500(25°-35°N,80°-120°E)} - \overline{U}_{500(50°-60°N,80°-120°E)} \quad (1)$$

where $\overline{U}_{500(25°-35°N,80°-120°E)}$ and $\overline{U}_{500(50°-60°N,80°-120°E)}$ are the mean values of 500 hPa zonal wind in their respective regions. The index is the normalized value.

Meridional index over Asia (I_M): we firstly divided the East Asian region (45–65° N, 60–150° E) into three areas (60–90° E, 90–120° E, 120–150° E), and then calculated I_M for each area according to formula (2):

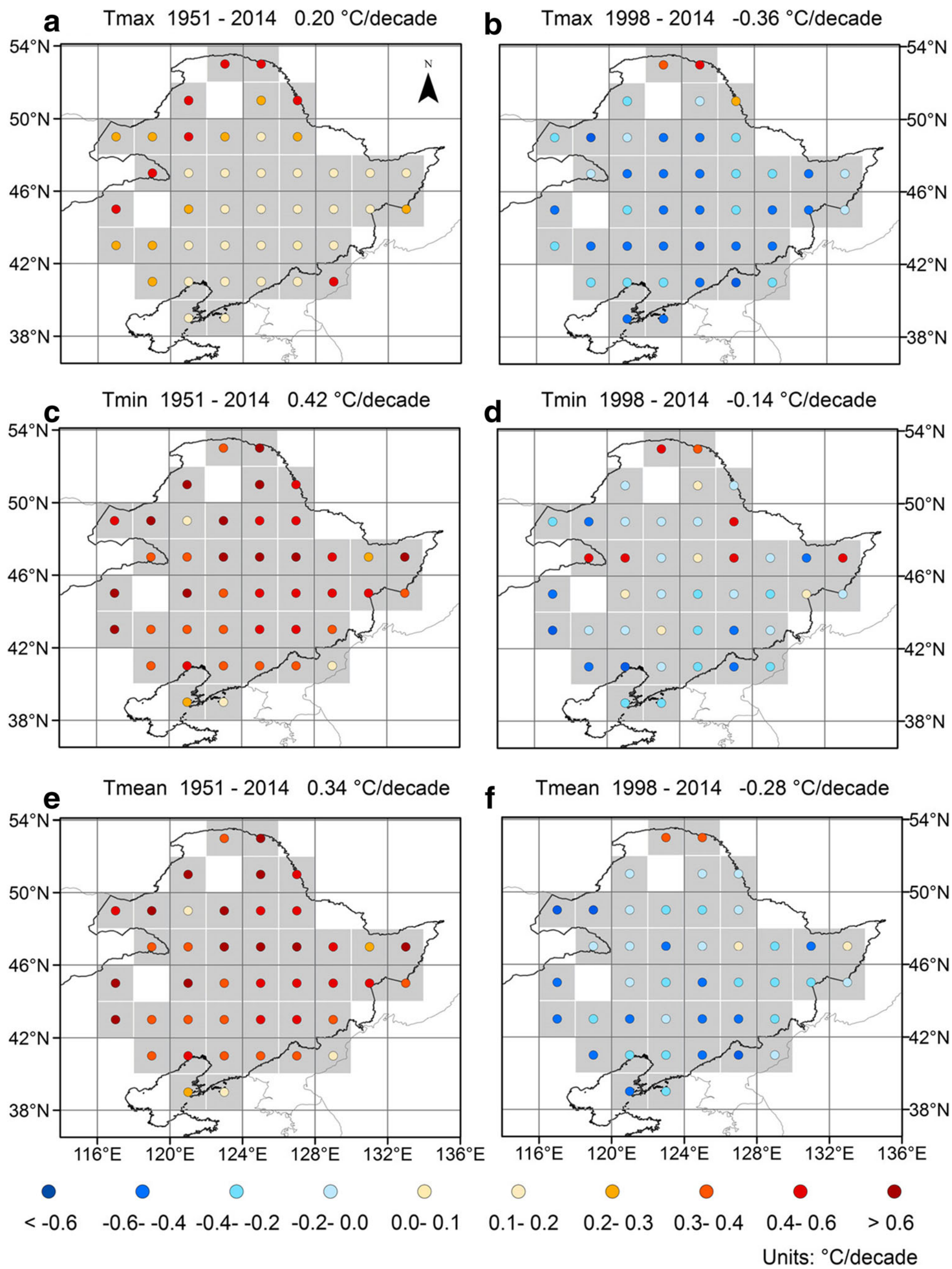

Fig. 3 Trends of Northeast China temperature in specific periods (1951–2014 and 1998–2014). Figure on the *left* shows the spatial distribution of the Tmax (**a**), Tmin (**c**) and Tmean (**e**) trends for 1951–201. Figure on the *right* shows the spatial distribution of the Tmax (**b**), Tmin (**d**) and Tmean (**f**) trends for 1998–2014.The details above each plot indicate the different periods and the trends of regional mean

$$I_M = \frac{1}{n}\sum_{j=1}^{n}\left|\overline{\left(\frac{1}{\cos\varphi}\frac{\partial z}{\partial\lambda}\right)_j}\right| = \frac{1}{n}\sum_{j=1}^{n}\left|\frac{1}{m}\sum_{i=1}^{m}\left(\frac{1}{\cos\varphi_j}\frac{\Delta z_i}{\Delta\lambda}\right)_j\right| = \frac{1}{mn\Delta\lambda}\sum_{j=1}^{n}\left|\left[\sum_{i=1}^{m}\left(\frac{\Delta z_i}{\cos\varphi_i}\right)\right]_j\right| \tag{2}$$

where n is the number of partitions within the study region; m is the number of φ (here $m = 3$); $\Delta\lambda = 15°$ longitude; φ_1, φ_2, and φ_3 are 45° N, 55° N, and 65°N respectively; and Δz_i is the difference between the height of every 15° ($\Delta\lambda$) longitude.

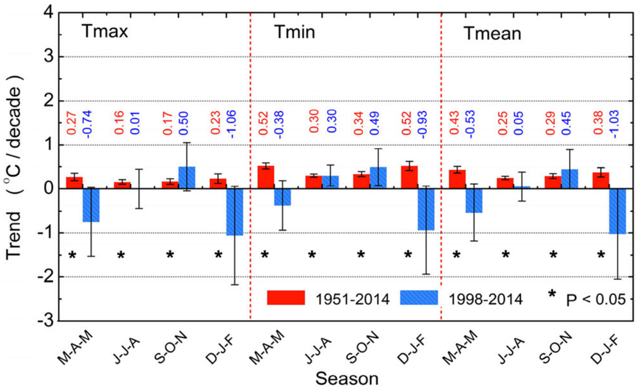

Fig. 4 Decadal trends (°C/decade, *red and blue bars*) of Tmax (*left*), Tmin (*middle*), and Tmean (*right*). Statistically significant (P < 0.05) trends are marked with *asterisks*. *Error bars* indicate two times the standard deviation

3 Results

3.1 Annual temperature changes

The annual mean time series of Tmax, Tmin, and mean temperature (Tmean) anomalies are shown in Fig. 2a–c. For the study period (1951–2014), annual mean temperature anomalies reflect significant positive trends (P < 0.05), and the warming rates of Tmax, Tmin, and Tmean are 0.20, 0.42, and 0.34 °C/decade, respectively, over the study region (red bars in Fig. 2a, b, c). The warming rate of Tmin is about twice that of Tmax, which suggests that the warming in recent decades can be attributed to stronger increases in Tmin. It is also clear that the warming trend of Tmean in the study region is larger than that of mainland China (Ren et al. 2005; Li et al. 2015) and global average (Jones et al. 2001). Based on the time series, we further found that 2007 was the warmest year in the study region since 1951. For the period 1951–1997, the warming rates of annual temperature are larger than that in whole study period (orange bars in Fig. 2a, b, c). The decadal mean of temperature anomalies are shown in Fig. 2d, which clearly indicates the inter-decadal variation in temperatures. The decadal mean anomalies of Tmin are slightly lower than those of Tmax before 1980, but considerably higher than Tmax after 1980. The anomaly of Tmin clearly increased from the late 1970s, while Tmax and Tmin significantly increased from the late 1980s. Previous studies have indicated that significant warming began at the majority of the stations in mainland China in the mid-1980s (Ren et al. 2005; Tang et al. 2005). All of the above analyses reveal that the significant warming occurred in the study region later than in most parts of China.

In the GWH period, annual temperatures show clear negative trends (blue bars in Fig. 2a–c). The cooling trends since 1998 in Tmax, Tmin, and Tmean respectively are −0.36, −0.14, and −0.28 °C/decade. These negative trends may be largely attributed to several cold years around 2010, particularly 2010 and 2012, as shown in Fig. 2a, b, c. Remarkably, all of the trends in the hiatus period are not significant (P < 0.05), with a higher level of uncertainty (black error bar in Fig. 2a, b, c), which can mainly be attributed to the short series length. Overall, a remarkable cooling phenomenon in the GWH period occurred over the study region, and Tmax showed more obvious cooling trends than Tmin and Tmean.

Spatial patterns of the decadal trends in temperature in the study region are shown in Fig. 3. From 1951 to 2014 (Fig. 3a–e), all of the grids consistently show a warming spatial pattern, however, with different warming rates. The warming rates of Tmin and Tmean were above 0.4 °C/decade, and the larger change occurred in the region of north of 46° N and the Mongolian Plateau. Although Tmax also exhibits widespread warming, the warming rate was considerably lower than Tmin and Tmean. The spatial pattern of Tmax indicates an increase in the warming rate of Tmax with altitude increase. This result is in agreement with Dong et al. (2015), who showed that the temperature trend increased from 200 to 2000 m with altitude increase.

In the GWH period, the majority of grid boxes exhibit widespread cooling trends, except some grid boxes in the north of the study region (Fig. 3b–f). Moreover, the trends of Tmax and Tmean show a wider cooling range than Tmin. More than ~90% of the grid boxes show decreasing trends in Tmax and Tmean, while ~30% of the grid boxes show warming trends of Tmin. In general, the above evidence suggests that the hiatus phenomenon that has occurred since 1998 can be more strongly attributed to the substantial decreases in Tmax than to decreases in Tmin.

3.2 Seasonal temperature changes

Decadal trends of seasonal temperature during the different periods are shown in Fig. 4. During 1951–2014 (Fig. 4 red bar), Tmax, Tmin, and Tmean consistently show significant warming trends (P < 0.05), and the warming rate in winter and spring are larger than in summer and autumn. The warming rate of Tmin was significantly higher than that of Tmax. In the GWH period (Fig. 4, blue bar), hiatus phenomena were observed in spring, summer, and particularly in winter with a winter cooling rate lower than −0.8 °C/decade. Conversely, the warming rate in autumn was higher relative to the recent 64 years. In general, the cooling trends of annual temperature in Northeast China were mainly controlled by the cooling trends in winter and spring during the GWH period, indicating that the warm and cold seasons have become more polarized. In addition, all the trends in the GWH period are associated with a higher level of uncertainty (black error bar in Fig. 4).

Spatial patterns of Tmean seasonal trends in the GWH period and the whole period are shown in Fig. 5. Because of the similar spatial distribution among Tmax, Tmin, and

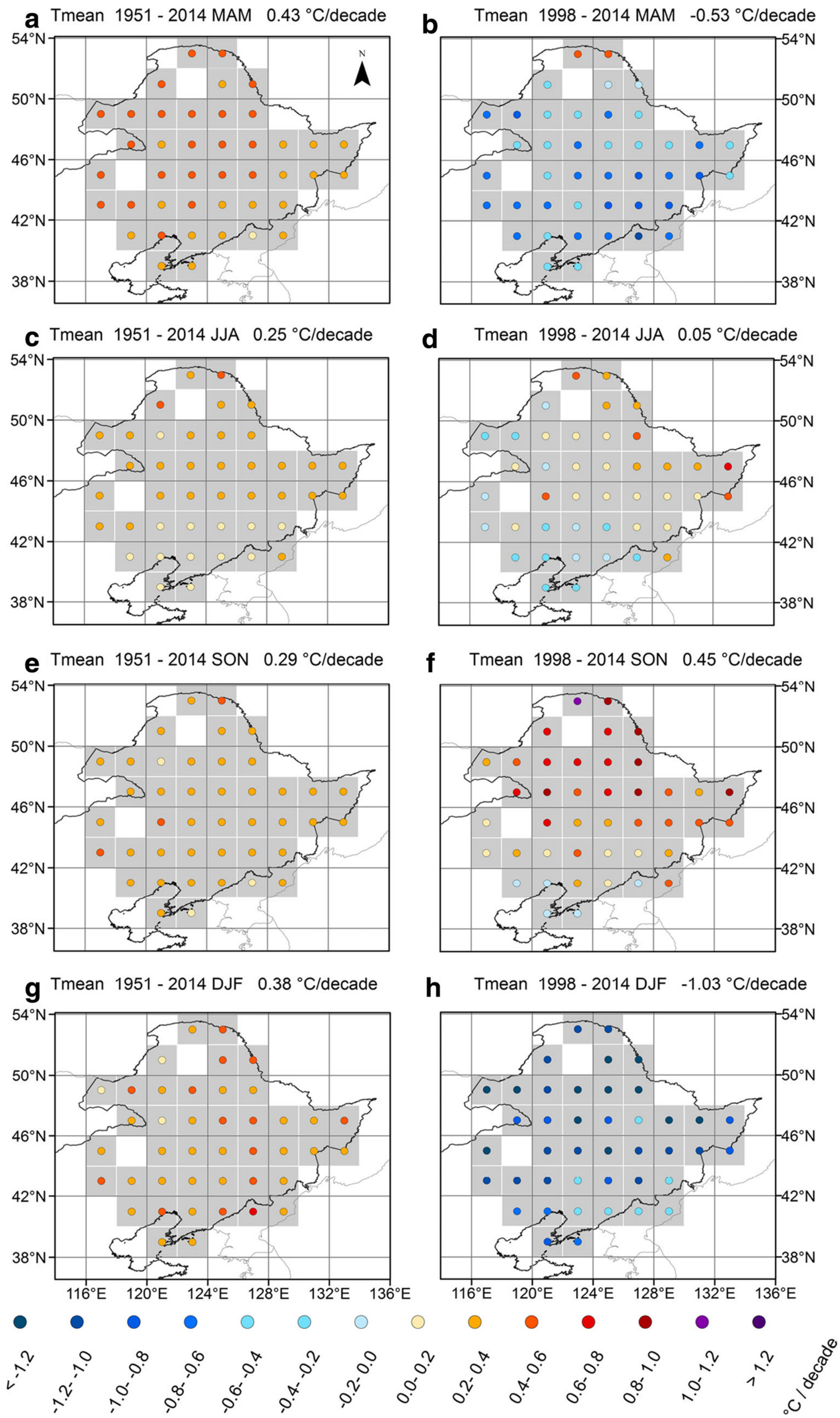

Fig. 5 Season trends of Northeast China Tmean change in specific periods (1951–2014 and 1998–2014). The details above each plot indicate the different periods and the trends of regional mean. Figure on the *left* (**a, c, e, g**) shows the season trends for 1951-2014. Figure on the *right* (**b, d, f, h**) shows the season trends for 1998-2014

Tmean, we discuss only the spatial pattern of Tmean. From 1951 to 2014, greater warming phenomenon in spring and winter occurred through most of the grid boxes. Conversely, in the GWH period, almost all of the warming grid boxes in

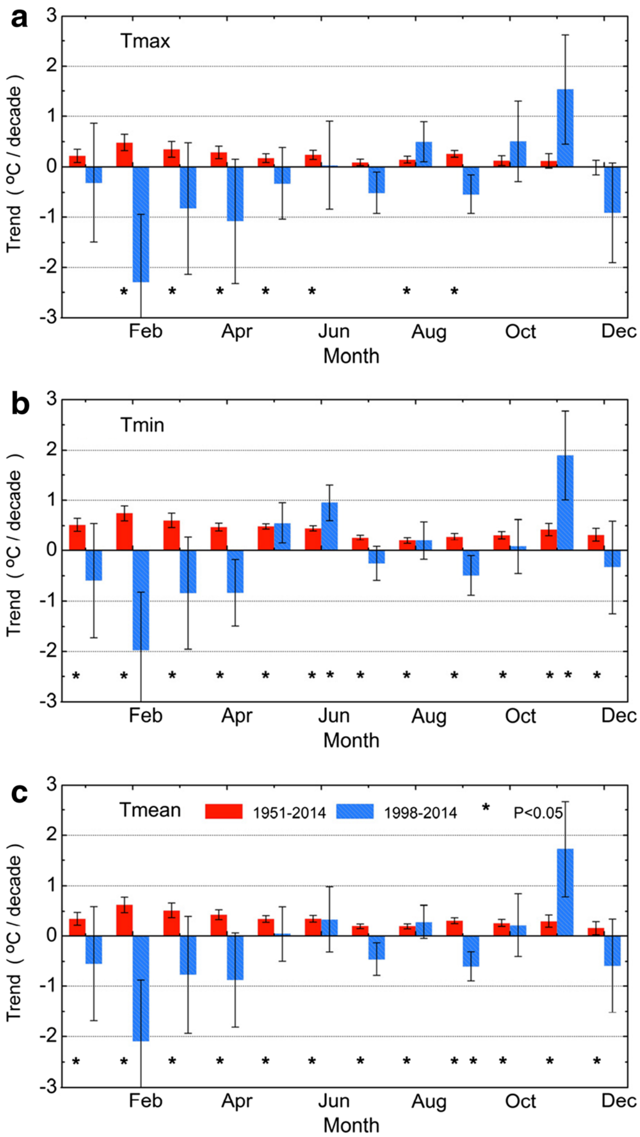

Fig. 6 Monthly trends (°C/decade, *red and blue bar*) of mean Tmax (**a**), Tmin (**b**), and Tmean (**c**). Statistically significant ($P < 0.05$) trends are marked with *asterisks*. *Error bars* indicate two times the standard deviation

the whole period showed cooling trends in spring and winter. The largest decrease of spring mean temperature occurred in central and southern parts of the study region. In summer and autumn of the GWH period, the trends increased from slight cooling to considerable warming with increased latitude. In autumn, the warming trends in the GWH period were considerably larger than in the past 64 years, especially in the areas north of 46° N.

3.3 Monthly temperature changes

Linear trends of monthly Tmax (a), Tmin (b), and Tmean (c) in the whole period and the GWH period are shown in Fig. 6. From 1951 to 2014, warming trends were observed in all months, and the warming rates during January to June were larger than those during July to December. February showed the largest warming trend and the lowest change usually occurred in December. During the GWH period, there were 7 months that consistently showed cooling trends, which is more than the warming months. The larger cooling trends mainly occurred from February to April, and the largest warming month was November. Moreover, all of the trends in the GWH period were associated with a high error level.

The spatial patterns of Tmean trends for February and November in the whole period (a, c) and the GWH period (b, d) are shown in Fig. 7. In the GWH period, the spatial distribution of November (d) and February (b) show opposite patterns. In February, all the grid boxes showed cooling trends with a cooling rate lower than −0.8 °C/decade. However, in November, all the grid boxes show greater warming trends especially north of 46° N where the warming rates even reached 2.0 °C/decade.

3.4 Comparison of the trends based on different trend estimator

We used Sen's slope and least squares estimator to assess the linear trends of the full study period (1951–2014) and the GWH period (1998–2014), and to compare the results based on the two methods. Table 1 shows the differences between Sen's slope trends and least squares trends. For the period 1951–2014, there are almost no differences on the trends obtained using the two estimation methods. The trends for hiatus period by using the Sen's slope method are slightly lower than that by using the least squares method, but all the results show consistent hiatus phenomenon over Northeast China (Table 1). For statistical significance, both of the two estimation methods show significant long-term trends for the entire period, and non-significant trends of the hiatus period. Therefore, the two methods have little impact on the estimated results of linear temperature trends and their significance over Northeast China, but the magnitudes of the trends do have slight differences, and this may call for a caution in estimating the temperature trends using the least squares method.

3.5 Comparison of Northeast China, mainland China, and global analyses

Table 2 gives the annual mean surface temperature trends in Northeast China (Section 3.1–3.3), mainland China (Li et al. 2015), and the global averages (Karl et al. 2015; Kosaka and Xie 2013). Because these studies used different datasets and base periods, it only shows an approximate comparison of the temperature trends.

Global analysis results suggested that the annual mean temperature increase was significant during 1998 to 2014 over the

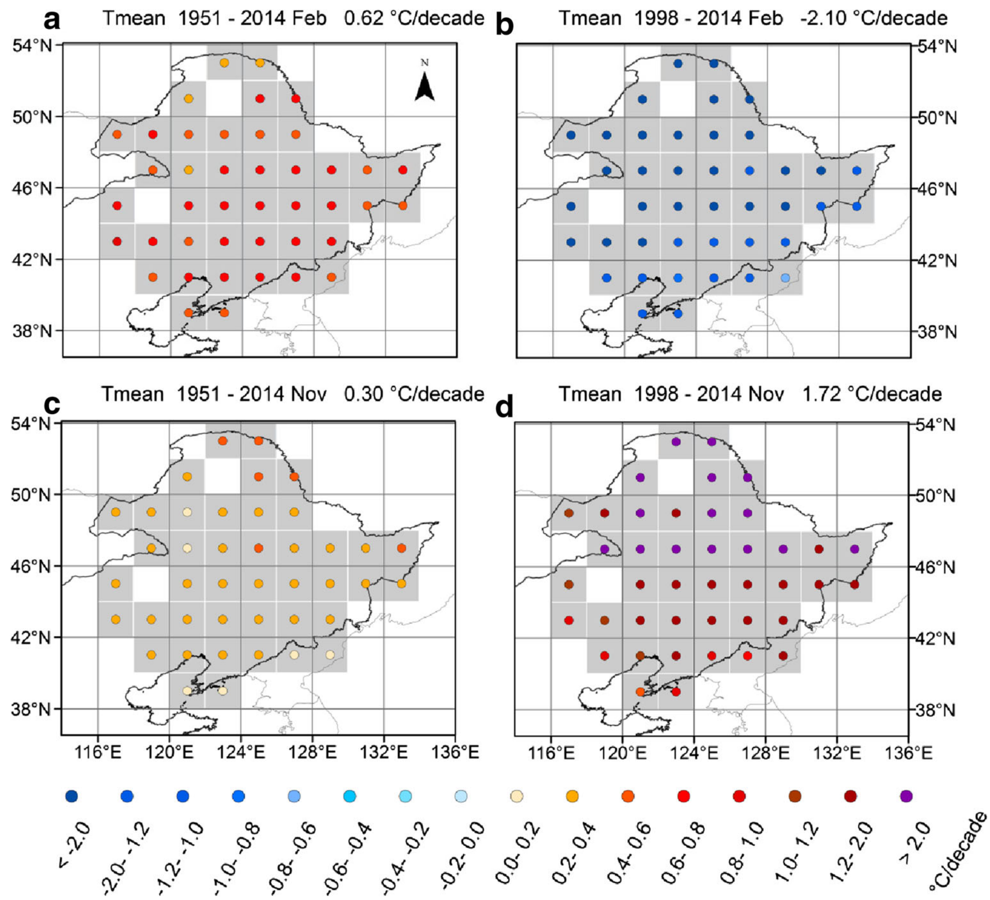

Fig. 7 Tmean trends of February (**a**, **b**) and November (**c**, **d**) temperature over Northeast China in specific periods (1951–2014 (**a**, **c**) and 1998–2014 (**b**, **d**). The *details above each plot* indicate the different periods and the trends of regional mean

global land surface (Karl et al. 2015). In Northeast China, however, the annual mean surface air temperature showed a cooling trend over the GWH period. This illustrates that there remains a remarkable hiatus phenomenon at the regional scale, in areas such as Northeast China. For the seasonal hiatus, the comparison between Northeast China and the globe (Kosaka and Xie 2013) reveals that both consistently showed cooling trends during DJF and MAM, and the season with the largest cooling trends was DJF. During JJA, global and Northeast China consistently showed warming trends. However, during SON, the global result showed a slight cooling trend, but Northeast China exhibited a greater warming trend.

Comparison of the temperature changes between mainland China (Li et al. 2015) and the study region for annual mean Tmax and Tmin indicated a better agreement in the GWH period, with both showing remarkable cooling trends. For seasonal analysis, the negative trends in Northeast China were larger than those in mainland China during MAM. During SON, the most significant difference between mainland China and Northeast China was in Tmax, and there was clear warming in Northeast China but slight cooling over mainland China. In general, this analysis illustrates that the hiatus phenomenon was more evident in Northeast China, and the cooling trends were clearer in the cold season.

4 Circulation anomaly during the GWH

Sections 3.2 and 3.3 indicated that the decreasing trend of annual mean temperature in Northeast China during the GWH period is mainly controlled by the cooling of winter and spring, especially the winter cooling. In this section, we further analyzed the relationship between the warming hiatus of winter over Northeast China with the atmospheric circulation anomaly in larger spatial scale.

EOF method was used to analyze the winter temperature of Northeast China during the period 1951–2014. The results showed that the first mode contribution was 80%, and the temperature in Northeast China region shows a spatially consistent change. This result is similar with the previous research by Fang et al. (2013). It shows that the winter temperature in Northeast China shows the characteristics of synchronous change.

We used SVD method to analyze the correlations of the winter mean temperature in Northeast China with the SLP field, the 500 hPa geopotential height field, and the 500 hPa zonal wind field. The variance contribution of SVD for SLP field, 500 hPa geopotential height field, and 500 hPa zonal wind field are 91, 90, and 85% in the first mode components, respectively, with the correlation coefficients of the

Table 1 Trends of temperature in different periods over Northeast China based on different trend estimation methods

Regions	Periods	Elements	Season MAM	Season JJA	Season SON	Season DJF	Annual
Northeast China	1951–2014	Tmax	0.29[a]	0.14[a]	0.16[a]	0.26[a]	0.19[a]
			0.27[a]	0.16[a]	0.17[a]	0.23[a]	0.20[a]
		Tmin	0.52[a]	0.28[a]	0.35[a]	0.56[a]	0.42[a]
			0.52[a]	0.30[a]	0.34[a]	0.52[a]	0.42[a]
		Tmean	0.45[a]	0.23[a]	0.28[a]	0.40[a]	0.34[a]
			0.43[a]	0.25[a]	0.29[a]	0.38[a]	0.34[a]
	1998–2014	Tmax	–0.70	–0.07	0.31	–1.07	–0.39
			–0.75	0.03	0.50	–1.06	–0.36
		Tmin	–0.43	0.33	0.26	–1.35	–0.09
			–0.37	0.30	0.50	–0.94	–0.14
		Tmean	–0.53	0.12	0.41	–1.30	–0.26
			–0.54	0.05	0.45	–1.03	–0.28

The red numbers represent Sen's slope trends, and the blue numbers represent least squares trends (unit: °C/decade)

[a] The trends are significant at the 5% level

normalized time coefficient series between the three fields and the winter temperature in Northeast China being 0.79, 0.7, and 0.78 ($P < 0.01$), respectively. These illustrate that there are good relationships between winter temperature and SLP field, 500 hP a geopotential height field, and 500 hPa zonal wind field.

The distribution map of heterogeneous correlation for SVD first mode between the winter temperature field in Northeast China and SLP field, 500 hPa geopotential height field (Fig. 8a, b) show that there are two significant correlation regions. The Arctic region shows a significant negative correlation, and the middle latitude regions show significant positive correlation. The two regions are remarkably related to the controlling area of AO and SH. The distribution of heterogeneous correlation between zonal wind field and the winter temperature field (Fig. 8c) shows that the two significant correlation regions are consistent with the regions used to define the EAWM index by Zhu et al. (2008).

Overall, all above analyses indicate that there are good relationships between AO, SH, EAWM, and the winter temperature in Northeast China. If AO is in its positive (negative) phase and at the same time SH and EAWM are stronger (weaker) than normal, the winter mean temperature will be anomalously warm (cold) over Northeast China. Besides, EAT is also an important system related to cold wave in Northeast China and is closely related to the EAWM (Ding et al. 2014). Several previous analyses of the EAT indicated that its strengthening (weakening) is always accompanied by cold (warm) winter in Northeast China (Chen et al. 2014; Leung and Zhou 2015a). At the same time, the mean position of the EAT can also influence the winter temperature of eastern China (Leung and Zhou 2015b).

Table 2 Comparison of Northeast China, mainland China (Li et al. 2015), and global (Karl et al. 2015; Kosaka and Xie 2013) temperature changes for the GWH period

Sources	Regions	Periods	Data sets	Methods	Elements	Season MAM	Season JJA	Season SON	Season DJF	Annual
Karl et al. (2015)	Global land-surf	1998–2014	ISTI Databank v1.0.0	Sen's slope	Tmean					↑
Kosaka and Xie. (2013)	ace	2002–2012	HadCRUT v 4.1.1.0	Sen's slope	Tmean	↓	↑	↓	↓	
Li et al. (2015)	Mainland China	1998–2012	China Homogenized Temperature Data set (CHTD)	Sen's slope	Tmax	↓	↑	↓	↓↓↓	↓↓
					Tmin	↓	↑↑	↑↑	↓↓↓	↓
					Tmean					
This paper	Northeast China	1998–2014	CHHTD-V1.0	Sen's slope	Tmax	↓↓↓	↓	↑↑↑	↓↓↓	↓↓
					Tmin	↓↓	↑↑	↑↑	↓↓↓	↓
					Tmean	↓↓↓	↑	↑↑	↓↓↓	↓↓

↓↓↓ <–0.5< ↓↓ <–0.25 < ↓ < 0.0 < ↑ < 0.25< ↑↑ < 0.5< ↑↑↑ °C/decade

The red (blue) arrows indicate increasing (decreasing) trends, and the number of arrows indicates the range of trend values (see the legend below the table)

ISTI Databank v1.0.0 International Surface Temperature Initiative Databank v1.0.0, *HadCRUT v 4.1.1.0* Hadley Centre-Climate Research Unit combined land surface air temperature v 4.1.1.0, *CHTD* China Homogenized Temperature Data set (total about 860 stations in China), *CHHTD-V1.0* China Homogenized Historical Temperature Data set-V1.0 (total 2419 stations in China)

These results are generally consistent with the previous studies (Sun and Li 2012; Li et al. (2013a, b); Ding et al. 2014; Liu et al. 2013a, b; Fang et al. 2013). Fig. 9 shows the decadal mean of temperature anomalies in Northeast China (a), mean position of the EAT (I_{EATS}) (b), EAT index (I_{EAT}) (c), Meridional Index (I_M) (d), AO index (I_{AO}) (e), SH index (I_{SH}) (f), and EAWM index (I_{EAWM}) (g) for DJF (the arrows represent increasing or decreasing trends). It is clear that all of the indices trends have reversed during the 1990s. During the 1990s, I_{EATS} was located in the Japan east Pacific (about 148°E), and the I_{EATS} and I_M were consistently in a weak state, limiting the cold air of the polar region from entering Northeast China, with a result of abnormal high winter mean temperature in the study area (Fig. 2a). Decadal mean values of 2000s showed that I_{EATS} moved westward to Japan (about 144° E), closer to Northeast China. Moreover, the I_{EAT} and I_M changed from weak phases in the 1990s to strong phases, AO changed to a negative phase, and SH, EAWM, EAT, and meridional wind are all consistently in their strong phases. The circulation abnormality benefited the more frequent bursts of the winter cold waves and the decrease of seasonal mean temperature in Northeast China during the GWH period.

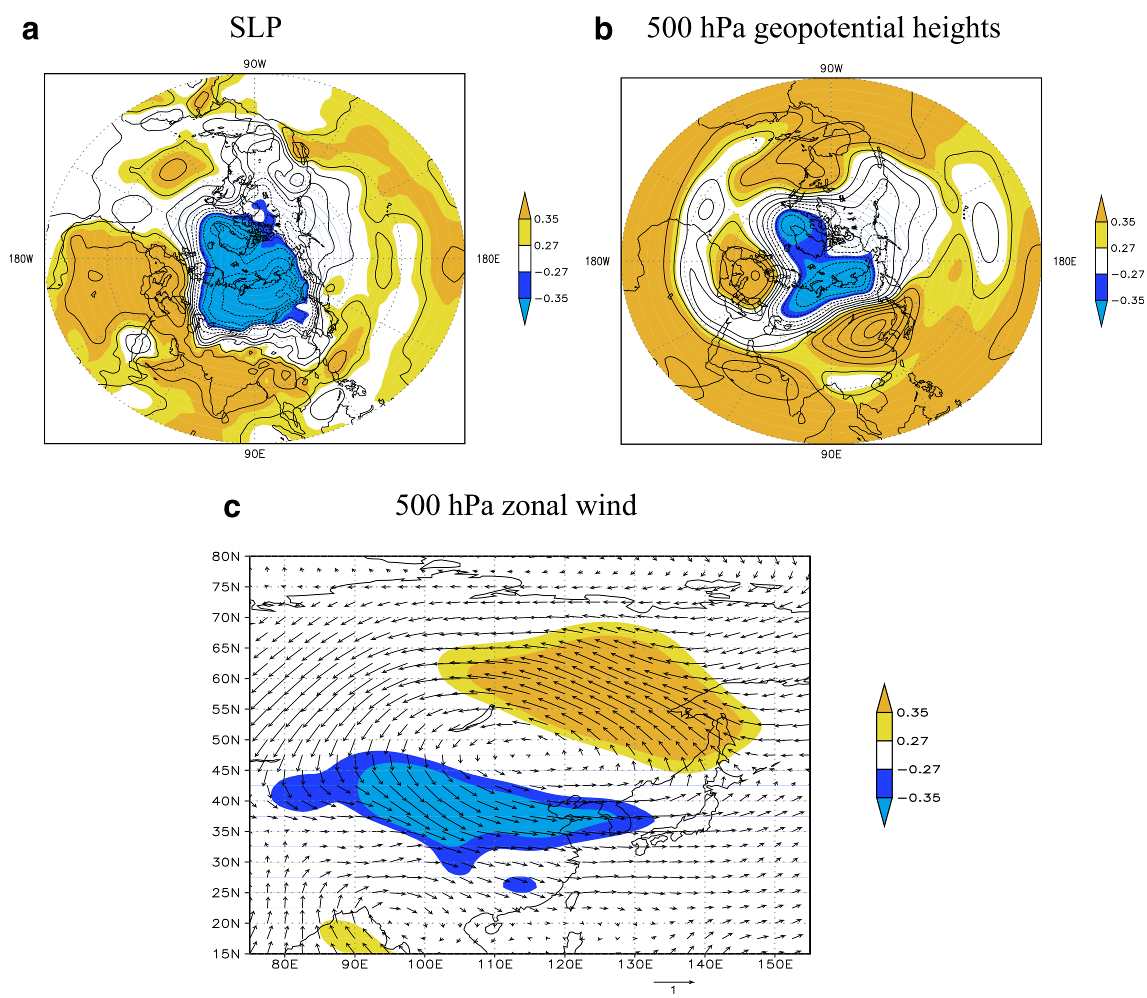

Fig. 8 The distribution of heterogeneous correlation for SVD first mode between the winter mean temperature field in Northeast China and SLP field (**a**), 500 hPa geopotential heights field (**b**), and 500 hPa zonal wind field (**c**). The *shaded areas* represent those with significant correlations, and ±*0.27* (±*0.35*) indicate that the correlations are significant at the 0.05 (0.01) level

Figure 10 shows a schematic diagram of the possible mechanism of winter warming hiatus phenomenon in Northeast China. The hiatus phenomenon appears under the background of negative AO and the stronger SH, EAWM, EAT, and meridional wind. Under the synergistic effects of the atmospheric circulation factors, the cold air of the polar region more easily moved into Northeast China, and the winter temperatures correspondingly experienced the cooling phenomenon.

5 Discussion

Most observational data used in this paper had a relatively long and high-quality record, especially after 1960. However, the station spatial coverage was poorer during 1951–1960. Therefore, the temperature anomalies calculated for earlier period (1951–1960) have a larger uncertainty. Furthermore, the poorer data coverage can also impact the long-term trend estimate (Brohan et al. 2006), leading to uncertainties of the trend values in the 1951–2014 period. However, the uncertainties of the trend estimates are relatively small by comparing the previous analyses of both the study region and mainland China. In addition, this work was focused on the GWH period, and the temperature trends during the whole time period could be regarded as a background change. In the last 50 and 20 years, the quality and spatial coverage of the data are better than the early data, so the bias from data could not substantially impact the final results.

Overall, our analysis result confirms a remarkable warming slowdown in Northeast China during the GWH period, and the hiatus is more obvious than those reported for mainland China and the globe. This is in a strong contrast to the fact that Northeast China had experienced the most significant warming in mainland China and East Asia by late 1990s (Hansen et al. 2006; Ren et al. 2012; Jones et al. 2012). It would be interesting to examine whether or not the other rapidly warming regions of the global lands also see a larger decline of surface air temperature during the GWH period.

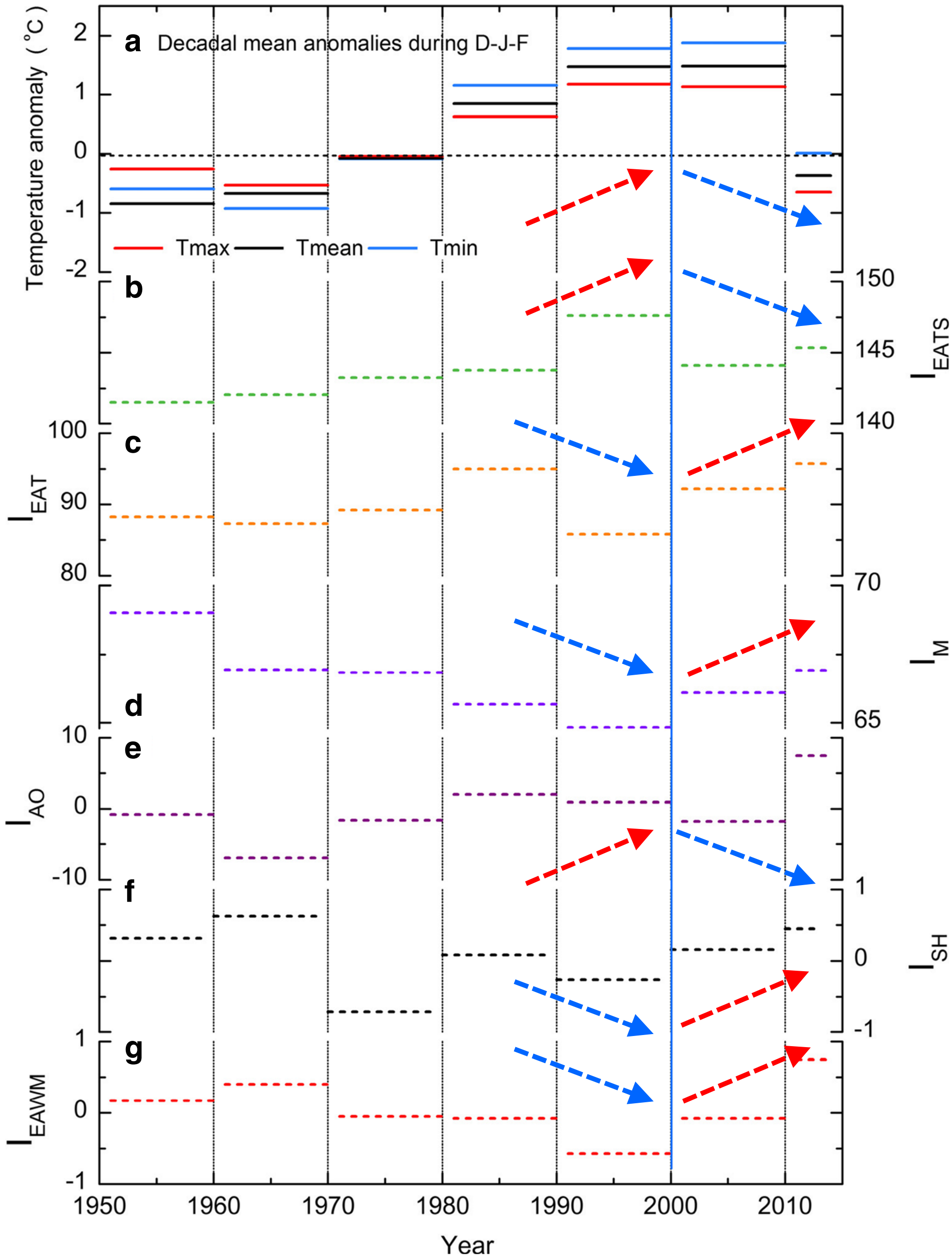

Fig. 9 Decadal mean of temperature anomalies of Northeast China (**a**, °C), I_{EATS} (**b**, °E), I_{EAT} (**c**), I_M (**d**), I_{AO} (**e**), I_{SH} (**f**), and I_{EAWM} (**g**) indices for DJF (the *arrows* represent increasing or decreasing trends)

In Section 4, the direct influential factors of the Northeast China temperature decline during the GWH period was investigated in terms of large-scale atmospheric circulation anomaly. We just founded out the factors of winter temperature change in Northeast China. In reality, however, there remains a complex physical mechanism between EAWM and the EAT (Leung et al. 2016), and studies have also indicated that a range of factors affecting the EAT and EAWM. Wu and Wang (2002) analyzed the winter AO, SH, and EAWM and indicated that, compared with impacts of the winter AO, the SH showed more direct and significant impacts on the EAWM and EAT, and this conclusion was confirmed by the other studies (e.g., Gong et al. 2001; Li and Wu 2012; Wu and Wang 2002; Sun and Li 2012). The negative temperature anomalies in the southern part of the EAT could also be reasonably explained by the phase of the El Niño–Southern Oscillation (ENSO) (e.g., Leung et al. 2016; Wang and He 2012; Zhou et al. 2013). Besides, Clark and Serreze (2000) found that snow depth and extents over land can affect the Pacific Ocean temperature and thus affect the EAT and EAWM. Recently, Qiao and Feng (2016) found that a significant positive correlation exists between the December NAO

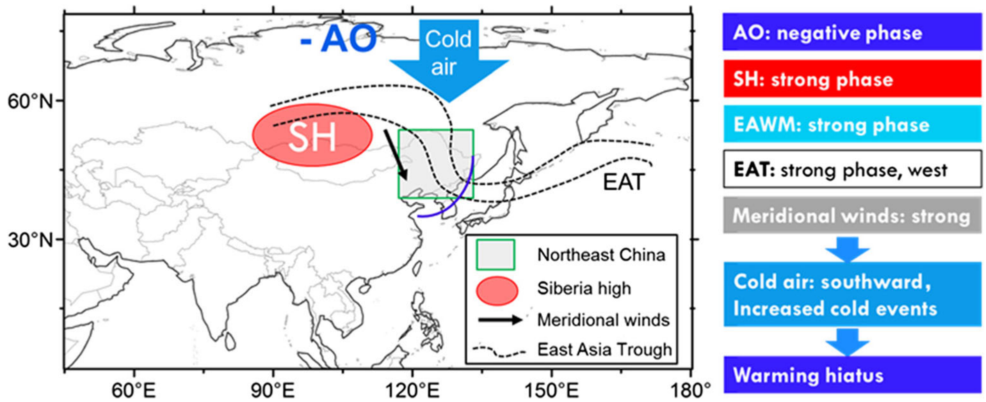

Fig. 10 A schematic diagram of the mechanism of winter warming hiatus phenomenon in Northeast China during 1998–2014

and the following February EAT, and much of China features cold anomalies with significant signals observed over northeastern China in strengthened EAT and NAO years. Huang et al. (2013) analyzed the variations of the intensity of EAT and indicated that the variation of EAT may be related to the eastward propagation of Rossby wave. Above studies illustrate that the physical mechanisms for the hiatus phenomenon in Northeast China are complex, and the interactions among the atmospheric, oceanic, and land surface factors and the fundamental mechanisms still require further examination.

Whatever the reason for the warming slowdown, the cooling climate in Northeast China during the past 17 years may pose a huge challenge to the agricultural activity and natural system. Northeast China plain is one of the most productive regions of grains in the world. The grain yield amounts to ~20% of China's total. The growth season here mainly concentrates in March–October, but the cold weather in spring and summer frequently causes loss of grain production in the region. Our analysis in Section 3 shows that the hiatus phenomenon is more evident in Northeast China especially in the cold season (MAM and DJF). The cooling trends in MAM signified that the accumulated temperature and heat conditions in the growth season may have worsen during the last two decades. It is worth noting if the cooling trend will continue in decades to come, with Li et al. (2013a, b), Sun et al. (2015), and others thought that it is very likely. If it will continue, the instability of agricultural production will increase in the future in this important grain production region of mainland China. This is especially anxious considering the widely hold expectation that climate will continue to become warmer in the decades to come without doubt in Northeast China.

It is also interesting to note that the phonological rhythms of a few plants seem to adjust to changed climate condition in Northeast China (Zhao 2016). An example comes from a species of willow and *Salix matsudana*, which has exhibited a delayed dates of leafing and flowering in spring since late 1990s (Zhao 2016). Obviously, further investigation is needed to examine the phonological and vegetation response of other species to the recent change in surface air temperature in Northeast China.

6 Conclusions

By applying observational data of monthly mean land surface Tmax, Tmin, and Tmean of 118 national stations since 1951, we investigated spatial and temporal pattern of temperature change for the periods 1951–2014 and 1998–2014 in Northeast China. Main conclusions can be drawn as follows:

(1) The increasing trends of Tmax, Tmin, and Tmean were 0.20, 0.42, and 0.34 °C/decade, respectively, over the period 1951–2014 in Northeast China, with the rate of Tmin about twice that of Tmax, and the upward trend of Tmean was clearly higher than the mainland China and global averages. The long-term warming occurred consistently across the study region, but the largest decrease of spring mean temperature mainly occurred in central and southern parts of Northeast China.

(2) In the GWH period, the annual mean temperature consistently exhibited a cooling trend in Northeast China, and the region-averaged annual trends of Tmax, Tmin, and Tmean were −0.36, −0.14, and −0.28 °C/decade, respectively.

(3) Seasonal mean temperature significantly decreased in winter and spring during the GWH period, but the warming was still evident in summer and autumn, indicating that the annual mean temperature decrease was mainly dependent on the remarkable winter and spring cooling in the study area.

(4) The monthly mean temperature series of Northeast China showed cooling trends in most months, with the largest decline occurring in February; however, the November mean temperature still showed a significant warming trend.

(5) Compared with the global and mainland China land surface temperature changes, the hiatus phenomenon in Northeast China was more evident, and the cooling trends were most evident in the cold season including winter and spring.

(6) The Northeast China cooling trend occurs in the time period of the negative phase Arctic Oscillation, and it is also closely related to strengthening of the SH and the EAT. The EAWM obviously becomes stronger over the GWH period as a result of the abovementioned changes in the circulation indices.

Acknowledgements This study is financed by the China Natural Science Foundation (CNSF) (Fund No: 41575003) and the Ministry of Science and Technology of China (MOST) (Fund No: GYHY201206012). The authors also thank two anonymous reviewers for their constructive comments.

References

Alexander LV, Zhang XB, Peterson TC, Caesar J, Gleason B, Klein Tank AMG, Haylock M, Collins D, Trewin B, Rahimzadeh F (2006) Global observed changes in daily climate extremes of temperature and precipitation. J Geophys Res Atmos 111(D5):1042–1063

An WL, Hou SG, Zhang WB, Wu SY, Xu H, Pang HX, Wang YT, Liu YP (2016) Possible recent warming hiatus on the northwestern Tibetan Plateau derived from ice core records. Sci Rep 6. doi:10.1038/srep32813

Balmaseda MA, Trenberth KE, Källén E (2013) Distinctive climate signals in reanalysis of global ocean heat content. Geophys Res Lett 40(9):1754–1759

Brohan P, Kennedy JJ, Harris I, Tett SFB, Jones PD (2006) Uncertainty estimates in regional and global observed temperature changes: a new data set from 1850. J Geophys Res Atmos 111(D12):121–133

Cao L, Zhu Y, Tang G, Yuan F, Yan Z (2016) Climatic warming in China according to a homogenized data set from 2419 stations. Int J Climatol 36:4384–4392. doi:10.1002/joc.4639

Carter B (2006) There is a problem with global warming... it stopped in 1998. Telegraph Newspaper (9 April 2006) (http://go.nature.com/D9CSlh).

Chen S, Chen X, Wei K, Chen W (2014) Vertical tilt structure of EAT and its interannual variation mechanism in boreal winter. Theor Appl Climatol 115(3):667–683

Chen X, Tung K (2014) Varying planetary heat sink led to global-warming slowdown and acceleration. Science 345(6199):897–903

Clark MP, Serreze MC (2000) Effects of variations in East Asian snow cover on modulating atmospheric circulation over the North Pacific Ocean. J Clim 13(20):3700–3710

Dong D, Huang G, Qu X, Tao W, Fan G (2015) Temperature trend-altitude relationship in China during 1963–2012. Theor Appl Climatol 122(1–2):285–294

Ding Y, Liu Y, Liang S, Ma XQ, Zhang Y, Dong SY, Liang P (2014) Interdecadal variability of the East Asian winter monsoon and its possible links to global climate change. J Meteorological Res 28(5): 693–713 (in Chinese)

Golub GH, Reinsch C (1970) Singular value decomposition and least squares solutions. Numer Math 14(5):403–420

Easterling DR, Wehner MF (2009) Is the climate warming or cooling? Geophys Res Lett 36(8):262–275. doi:10.1029/2009GL037810

Fang YH, Zhou F, Zhang YF, Zhao ZQ, Shen QY, Wang YS, Wang CX (2013) The comparison of factors on interannual and interdecadal variations of the winter temperature in Northeast China. Sci Geogr Sin 33(7):844–850 (in Chinese)

Franzke CL (2014) Warming trends: nonlinear climate change. Nat Clim Chang 4(6):423–424

Fyfe JC, Gillett NP (2014) Recent observed and simulated warming. Nat Clim Chang 4(3):150–151

Fyfe JC, Meehl GA, England MH, Mann ME, Santer BD, Flato GM, Hawkins E, Gillett NP, Xie SP, Yu K (2016) Making sense of the early-2000s warming slowdown. Nat Clim Chang 6(3):224–228

Gong DY, Wang SW, Zhu JH (2001) East Asian winter monsoon and Arctic oscillation. Geophys Res Lett 28(10):2073–2076

Hansen J, Sato M, Ruedy R, Lo K, Lea DW, Medina-Elizade M (2006) Global temperature change. Proc Natl Acad Sci 103(39):14288–14293

Hansen J, Sato M, Kharecha P, Schuckmann KV (2011) Earth's energy imbalance and implications. Atmos Chem Phys 11(24):13421–13449

Huang XM, Guan ZY, Dai ZJ, Mei HX (2013) A further look at the interannual variations of East Asian trough intensity and their impacts on winter climate of China. Acta Meteorol Sin 71(3):416–428

IPCC (2013) Climate change 2013: the physical science basis. In: Stocker TF, Qin D, Plattner G-K, Tignor M, Allen SK, Boschung J, Nauels A, Xia Y, Bex V, Midgley PM (eds) Contribution of working group I to the fifth assessment report of the intergovernmental panel on climate change. Cambridge University Press, Cambridge and New York, p 1535. doi:10.1017/CBO9781107415324

Jin ZQ, Ge DK, Shi CL, Gao LZ (2002) Several strategies of food crop production in the Northeast China Plain for adaptation to global climate change: a modeling study. Acta Agron Sin 28(1):24–31 (in Chinese)

Jones PD, Osborn TJ, Briffa KR, Folland CK, Horton EB, Alexander LV, Parker DE, Rayner NA (2001) Adjusting for sampling density in grid box land and ocean surface temperature time series. J Geophys Res Atmos 106(D4):3371–3380

Jones PD, Lister DH, Osborn TJ et al (2012) Hemispheric and large-scale land-surface air temperature variations: an extensive revision and an update to 2010. J Geophys Res 16(2):206–223. doi:10.1029/2011JD017139

Kerr RA (2009) What happened to global warming? Scientists say just wait a bit. Science 326(5949):28–29

Kosaka Y, Xie SP (2013) Recent global-warming hiatus tied to equatorial Pacific surface cooling. Nature 501(7467):403–407

Karl TR, Arguez A, Huang B, Lawrimore JH, Mcmahon JR, Menne MJ, Peterson TC, Vose RS, Zhang HM (2015) Possible artifacts of data biases in the recent global surface warming hiatus. Science 348(6242):1469–1472

Lorenz EN (1956) Statistical forecasting program: empirical orthogonal functions and statistical weather prediction. Sci Rep 409(2):997–999

Lathauwer LD, Moor BD, Vandewalle J (2000) A multilinear singular value decomposition. Siam J Matrix Analysis Applications 21(4): 1253–1278

Lean JL, Rind DH (2009) How will Earth's surface temperature change in future decades? Geophys Res Lett 36(15). doi:10.1029/2009GL038932

Lobell DB, Schlenker W, Costa-Roberts J (2011) Climate trends and global crop production since 1980. Science 333(6042):616–620

Li JP, Wu ZW (2012) Importance of autumn Arctic sea ice to northern winter snowfall. Proc Natl Acad Sci 109(109):E1898

Liu Z, Yang X, Chen F, Wang E (2013b) The effects of past climate change on the northern limits of maize planting in Northeast China. Clim Chang 117(4):891–902

Li JP, Sun C, Jin FF (2013b) NAO implicated as a predictor of Northern Hemisphere mean temperature multidecadal variability. Geophys Res Lett 40(20):5497–5502

Li WJ, Li Y, Chen LJ, Zhao ZG (2013a) Inter-decadal variability of the relationship between winter temperature in China and its impact factors. J Appl Meteorological Sci 24(4):385–396 (in Chinese)

Liu S, Sui B, Tu G, Feng XY (2013a) The East Asian winter monsoon background on the variation of winter air temperature in Northeast China. J Appl Meteorological Sci 25(1):11–21 (in Chinese)

Li QX, Yang S, Xu WH, Wang XL, Jones P, Parker D, Zhou L, Feng Y, Gao Y (2015) China experiencing the recent warming hiatus. Geophys Res Lett 42(3):889–898

Leung YT, Zhou W (2015a) Variation of circulation and East Asian climate associated with anomalous strength and displacement of the EAT. Clim Dyn 45(9–10):1–20

Leung YT, Zhou W (2015b) Vertical structure, physical properties, and energy exchange of the EAT in boreal winter. Clim Dyn 45(5–6): 1635–1656

Leung YT, Cheung HHN, Zhou W (2016) Meridional displacement of the EAT and its response to the ENSO forcing. Clim Dyn:1–18. doi:10.1007/s00382-016-3077-8

Meehl GA, Hu A, Arblaster JM, Fasullo J, Trenberth KE (2013) Externally forced and internally generated decadal climate variability associated with the Interdecadal Pacific Oscillation. J Clim 26(18):7298–7310

Qiao SB, Feng GL (2016) Impact of the December North Atlantic Oscillation on the following February EAT. J Geophys Res Atmos 121. doi:10.1002/2016JD025007

Ren GY, Ding YH, Zhao ZC, Zheng JY, Wu TW, Tang GL, Xu Y(2012) Recent progress in studies of climate change in China. Adv Atmos Sci 29(5):958–977

Ren GY, Guo J, Xu MZ, Chu ZY, Zhang LN, Zou XK, Li QX, Liu XN (2005) Climate changes of mainland china over the past half century. J Meteorological Res 63(6):942–956 (in Chinese)

Sen PK (1968) Estimates of the regression coefficient based on Kendall's tau. J Am Stat Assoc 63(324):1379–1389

Solomon S, Rosenlof KH, Portmann RW, Daniel JS, Davis SM, Sanford TJ, Plattner G (2010) Contributions of stratospheric water vapor to decadal changes in the rate of global warming. Science 327(5970): 1219–1223

Solomon S, Daniel JS, Neely RR, Vernier J, Dutton EG, Thomason LW (2011) The persistently variable "background" stratospheric aerosol layer and global climate change. Science 333(6044):866–870

Sun C, Li JP (2012) Analysis of anomalously low surface air temperature in the Northern Hemisphere during 2009/2010 winter. Clim Environ Res 17(3):259–273 (in Chinese)

Santer BD, Bonfils C, Painter JF, Zelinka MD, Mears C, Solomon S, Schmidt GA, Fyfe JC, Cole JN, Nazarenko L (2014) Volcanic contribution to decadal changes in tropospheric temperature. Nat Geosci 7(3):185–189

Seneviratne SI, Donat MG, Mueller B, Alexander LV (2014) No pause in the increase of hot temperature extremes. Nat Clim Chang 4(3):161–163

Sun C, Li JP, Jin FF (2015) A delayed oscillator model for the quasi-periodic multidecadal variability of the NAO. Clim Dyn 45:2083–2099. doi:10.1007/s00382-014-2459-z

Sun Y, Zhang XB, Ren GY, Zwiers FW, Hu T (2016) Contribution of urbanization to warming in China. Nat Clim Chang. doi:10.1038/nclimate2956

Sun XB, Ren GY, Xu WH, Li QX, Ren YY (2017) Global land-surface air temperature change based on the new CMA GLSAT dataset. Sci Bull 62(4):236–238

Thompson DWJ, Wallace JM (1998) The Arctic oscillation signature in the wintertime geopotential height and temperature fields. Geophys Res Lett 25(9):1297–1300

Tang HY, Zhai PM, Wang ZY (2005) On change in mean maximum temperature minimum and diurnal range in china during 1951–2002. Clim Environ Res 10(4):728–735 (in Chinese)

Tang GL, Luo Y, Huang JB, Wen XY, Zhu YN, Zhao ZC, Wang SW (2012) Continuation of the global warming. Adv Clim Chang Res 8(4):235–242 (in Chinese)

Tollefson J (2014) Climate change: the case of the missing heat. Nature 505(7483):276–278

Trenberth KE, Fasullo JT, Balmaseda MA (2014a) Earth's energy imbalance. J Clim 27(9):3129–3144

Trenberth KE, Fasullo JT, Branstator G, Phillips AS (2014b) Seasonal aspects of the recent pause in surface warming. Nat Clim Chang 4(10):911–916

Wu BY, Wang J (2002) Winter arctic oscillation, siberian high an East Asian winter monsoon. Geophys Res Lett 29:1897. doi:10.1029/2002GL015373

Wang H, He S (2012) Weakening relationship between East Asian winter monsoon and ENSO after mid-1970s. Chin Sci Bull 57:3535–3540

Yan L, Liu X (2014) Has climatic warming over the Tibetan Plateau paused or continued in recent years? Journal of Earth. Ocean Atmos Sci 1(1):13–28

Zhu YF, Tan GR, Wang YG (2008) An index of East Asian winter monsoon applied to description the Chinese mainland winter temperature changes. Acta Meteor Sin 66(5):781–788 (in Chinese)

Zhou Q, Wen C, Wen Z (2013) Solar cycle modulation of the ENSO impact on the winter climate of East Asia. J Geophys Res Atmos 118(118):5111–5119

Zhao CY (2016) Characteristics and long-term trend of plant phonology in Northeast China. A Ph.D. thesis of the Nanjing University of Information Science &Technology, Nanjing, China.

Zhao S, Li JP, Sun C (2016) Decadal variability in the occurrence of wintertime haze in central eastern China tied to the Pacific Decadal Oscillation. Sci Rep 6:27424. doi:10.1038/srep27424